Physical and Mechanical Behavior of Single-Walled Carbon Nanotube/Polypropylene/Ethylene–Propylene–Diene Rubber Nanocomposites

L. Valentini,[1] J. Biagiotti,[1] J. M. Kenny,[1] M. A. López Manchado[2]

[1]*Materials Engineering Center, Università di Perugia, 05100 Terni, Italy*
[2]*Instituto de Ciencia y Tecnologia de Polímeros, C.S.I.C. C/Juan de la Cierva, 3 28006 Madrid, Spain*

Received 1 August 2002; accepted 17 November 2002

ABSTRACT: The effects of the incorporation of single-walled carbon nanotubes (SWNTs) on the physical and mechanical properties of thermoplastic elastomers based on blends of isotactic polypropylene (iPP) and ethylene–propylene–diene rubber (EPDM) are described. A marked decrease of the half-time of PP–EPDM crystallization and a sensible increase of the overall crystallization rate were observed in the presence of SWNTs. These results confirmed the expected nucleant effect of nanotubes on the crystallization of polypropylene. This effect was not linearly dependent on the SWNTs' content, showing a saturation of the nucleant effect at high nanotube concentrations. Dynamic mechanical analysis results showed a significant and controversial change of the mechanical behavior of the PP–EPDM/SWNT composites depending on the nanotube content. In particular, the storage modulus increased at the lowest incorporation of SWNTs, whereas a further increase of nanotubes led to a reduction of the storage modulus with respect to the pristine polymer matrix. Raman spectroscopy and scanning electron microscopy were successfully applied to demonstrate that in the composite films, the changes in the crystallization kinetics and mechanical properties could be explained in terms of the changes of the distance between nanotubes in bundles after a different intercalation of the polymer matrix. J Appl Polym Sci 89: 2657–2663, 2003

Key words: matrix; nanocomposites; Raman spectroscopy; crystallization; mechanical properties

INTRODUCTION

The discovery of carbon nanotubes (CNTs) and carbon nanostructured materials has inspired scientists for a range of potential applications.[1–4] More specifically, the use of carbon nanotubes in polymer/carbon nanotube composites has attracted wide attention.[5,6] Carbon nanotubes have a unique atomic structure with a very high aspect ratio, as directly measured by transmission electron microscopy,[7] and extraordinary mechanical properties (strength and flexibility), making them ideal reinforcing fibers in nanocomposites. In this sense, it has been reported that the addition of CNTs in different polymer matrices have effectively enhanced the matrix properties.[8,9]

Among the most versatile polymer matrices, polyolefins such as polypropylene (PP) are the most widely used thermoplastics because of their well-balanced physical and mechanical properties and their easy processability at a relatively low cost that makes them a versatile material.[10–14] The toughening of PP by rubbers, particularly ethylene–propylene copolymers and terpolymers (EPM and EPDM, respectively), was found to be highly effective. These blends, commonly called thermoplastic elastomer polyolefins (TPOs), are a class of materials that combine the good processing characteristics of thermoplastics at elevated temperatures[15] with the physical properties of conventional elastomers at service temperatures,[16,17] playing an increasingly important role in the polymer industry. It is expected that the incorporation of reinforcing agents such as nanotubes will allow an improvement of some of the properties of these systems.

The main goal of this work was to analyze the combined effects of single-walled carbon nanotubes (SWNTs) on the morphology of PP–EPDM blends and to evaluate the physical and mechanical properties by varying the SWNT concentration. Thermal characterization was performed by means of differential scanning calorimetry (DSC). The mechanical behavior of the composites was studied using a dynamic mechanical analyzer. Finally, the vibrational and structural properties of the composites with several nanotube concentrations were studied by Raman spectroscopy and scanning electron microscopy.

EXPERIMENTAL

Commercially available grades of isotactic polypropylene (iPP; melt flow index 2.9 dg/min at 190°C and

Correspondence to: J. Kenny (kenny@unipg.it).

Journal of Applied Polymer Science, Vol. 89, 2657–2663 (2003)

5 kg; density 0.90 g/cm^3), kindly supplied by Solvay (Brussels, Belgium), and ethylene–propylene–diene rubber (EPDM) with 5-ethylidene-2-norbornene (ENB) as a termonomer (68% ethylene content, Mooney viscosity 55, ML_{1+8} of 23 at 125°C, and density 0.86 g/cm^3) supplied by Bayer (Germany) (trade name Buna EP T 6470 P) were used in this work. SWNTs were commercially obtained from CarboLex (Kentucky). The material consisted of packed bundles of SWNTs (12–20 Å in diameter). There were approximately 30 nanotubes per bundle (with an average bundle diameter of 100 Å) with a length of several micrometers.

To obtain the composite, 70 wt % PP and 30 wt % EPDM were melt blended with the addition of several nanotube concentrations specified as the wt % in the polymer: 0.25, 0.5, 0.75, and 1%. Three samples for each concentration were produced. The temperature of the mixing system was estimated by a thermocouple regulation to 190°C and the blending time was 10 min.

Thermal analysis measurements were performed using a DSC Mettler Toledo (model 822) differential scanning calorimeter. Crystallization tests were carried out both in isothermal conditions at 132°C and in dynamic conditions at a cooling rate of 10°C/min. For the isothermal testing, samples of about 5 mg were melted at 200°C for 10 min to eliminate any previous thermal history in the material. Then, they were rapidly cooled to the crystallization temperature (T_c; in our case, 132°C) and maintained at that temperature for the period necessary to complete the crystallization of the matrix. The heat evolved during the isothermal crystallization (ΔH_c) was recorded as a function of time. The experiments were carried out in a nitrogen atmosphere and after the isothermal crystallization test, a dynamic scan at 10°C/min was performed to check the presence of residual crystallinity. The degree of crystallization curves were constructed by integrating the area under the exothermic peaks.

For dynamic DSC testing, samples of about 5 mg were melted at 200°C for 10 min to eliminate any thermal history in the material. To confirm the thermal properties of the composites, at least three samples for each concentration of SWNTs were prepared and tested. Samples were subsequently cooled to 0°C at a scan rate of 10°C/min. Subsequently, the melting temperatures (T_m) of the blends were calculated as those corresponding to the maximum of the endothermic peak.

The dynamic mechanical properties of the composites were determined with a Metravib viscoelasticimeter (Mark 03 model). The nominal dimensions of the specimen were 25 × 5 × 0.5 mm. Tests were carried out in a torsion deformation mode at a frequency of 5 Hz and the temperature programs were run from −80 to 40°C under a sinusoidal strain, controlled at a heating rate of 2°C/min in a flow of nitrogen. An oscillating dynamic strain of 0.15% was used. To validate the experimental data reproducibility, three tests for each sample were carried out.

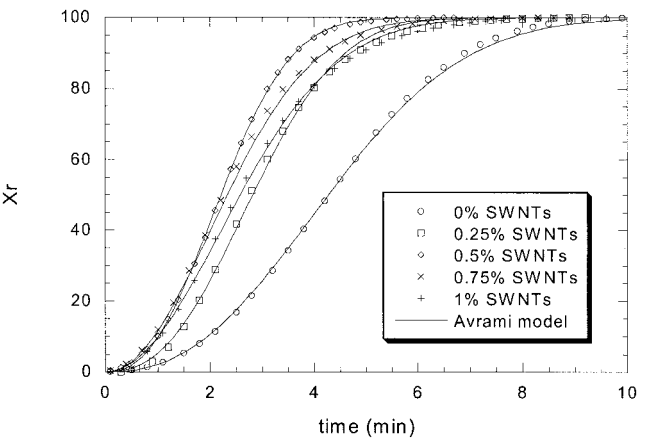

Figure 1 Isothermal crystallization curves of PP–EPDM/SWNT composites at 132°C.

Raman scattering spectra were recorded by a Jobin Yvon micro-Raman LabRam system in a backscattering geometry. A 632.8-nm (1.96-eV) He–Ne laser was used as the light source and optical filters adjusted the power of the laser. By using a 100× objective lens, the illuminated spot on the sample surface was focused to about 2 μm in diameter. The resolution of the Raman spectra was better than 1 cm^{-1}. Scanning electron microscopy (SEM) studies were performed on a Philips XL30 ESSEM operated at 15 kV.

RESULTS AND DISCUSSION

To analyze the effects of the incorporation of SWNTs on PP crystallization in the PP–EPDM blends, the relative degree of crystallization curves as a function of the time, obtained at 132°C, are represented in Figure 1. It can be observed that the PP crystallization rate increases when the SWNTs are added to the composite, in other words, the SWNTs behave as an effective nucleant agent for PP. It is of interest to note that this effect increases when increasing the SWNT content to reach a maximum for the composite with 0.5% of SWNTs. Further SWNT percentages produce a negative effect, showing a decrease of the PP crystallization rate, although they always remain above the corresponding values of the plain polymer. This behavior is also clearly reflected in analysis of the half-time of crystallization ($\tau_{1/2}$), reported in Table I. It is observed that $\tau_{1/2}$ decreases when SWNTs are incorporated into the nanocomposite, showing a minimum for the composite containing 0.5% SWNTs.

This particular behavior could be explained through the balance of the two opposite contributions. On the one hand, the results obtained suggest an increase of

TABLE I
Crystallization Temperature (T_c), Melting Temperature (T_m), Crystallization Enthalpy (ΔH), and Crystallization Kinetic Parameters of PP–EPDM and PP–EPDM/SWNT Composites

Composite	T_c (°C)	ΔH_c (J/g)	X_c (%)	T_m (°C)	n	K_n (min^{-n})	$\tau_{1/2}$ (min)	ΔH_c (J/g)
PP–EPDM	118.1	−39.63	27.1	161.2	2.46	1.94×10^{-2}	4.28	−41.13
PP–EPDM–0.25% SWNT	121.7	−64.44	44.8	163.4	2.46	5.24×10^{-2}	2.82	−48.66
PP–EPDM–0.5% SWNT	122.2	−64.97	44.4	163.7	2.35	1.09×10^{-1}	2.21	−55.12
PP–EPDM–0.75% SWNT	121.7	−65.13	44.9	163.5	2.01	1.34×10^{-1}	2.33	−47.06
PP–EPDM–1% SWNT	121.7	−58.70	40.1	163.5	2.00	1.02×10^{-1}	2.58	−32.29

nucleation at the nanotubes–matrix interface with the SWNTs content, whereas on the other hand, the same SWNTs could be responsible for the impingement effect on spherulitic growth.

A kinetic analysis was performed by applying the Avrami model to the results of the isothermal crystallization processes, accordingly to the following equation:

$$\chi_r(t) = 1 - \exp(-Kt^n)$$

where χ_r is the relative degree of crystallization, n is the Avrami exponent, K_n is the kinetic constant, and t is the crystallization time. K and n values, calculated by plotting $\log[-\text{Ln}(1 - \chi_r)]$ versus $\log(t)$ (Fig. 2) are reported in Table I. In all cases, fractional values of n were obtained and can be explained in terms of a partial overlapping of primary nucleation and crystal growth. Following the evident parallelism of Avrami plots, n values lie in a relatively narrow interval ($2 < n < 3$) and are traditionally attributed to a heterogeneous nucleation, followed by diffusion-controlled spherulitic crystalline growth. The values of the crystallization kinetic constant K_n confirm the inferred conclusions from the analysis of $\tau_{1/2}$ values, that is, that the PP crystallization rate is higher in the presence of the SWNTs, showing a maximum for composites with a 0.5% SWNT content.

The effects of SWNTs on the crystallization of the iPP in PP–EPDM blends were also analyzed in nonisothermal experiments. Figure 3 shows the relative degree of crystallization computed by the integration of the dynamic thermograms for all the studied composites. The observed dynamic crystallization behavior confirms the results obtained in isothermal tests regarding the positive effect of SWNTs on the crystallization kinetics of PP. The average values of the absolute degree of crystallization (X_c), the crystallization peak (T_c), and the apparent melting temperatures of the crystallized samples (T_m) are reported in Table I. These results show that the crystallization temperature increases when SWNTs are incorporated into polymer blends, an effect that is more evident for the composite containing 0.5% SWNTs. No substantial differences were observed on the melting temperature of the PP.

Figure 4 shows the SEM images of neat PP–EPDM and both 0.5 and 1% PP–EPDM/SWNT composites. In the 0.5% concentration sample [Fig. 4(b)], we notice a more uniform distribution of the bundles with a small quantity of aggregates. For the concentration of 1% [Fig. 4(c)], one can see an aggregate in which is observed a large amount of SWNTs self-organized in bundles.

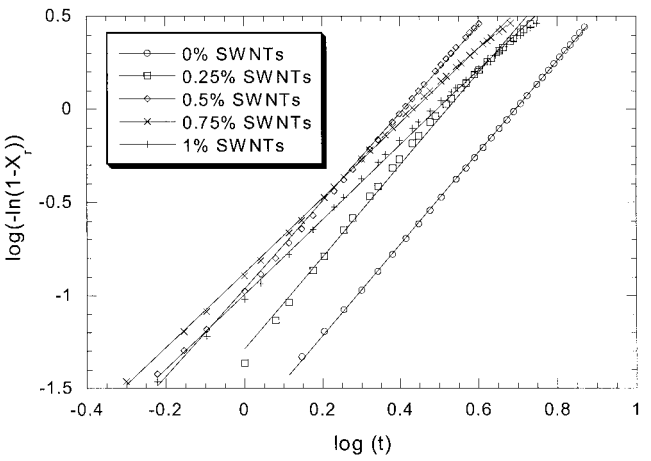

Figure 2 Avrami plots of neat PP–EPDM and PP–EPDM/SWNT composites.

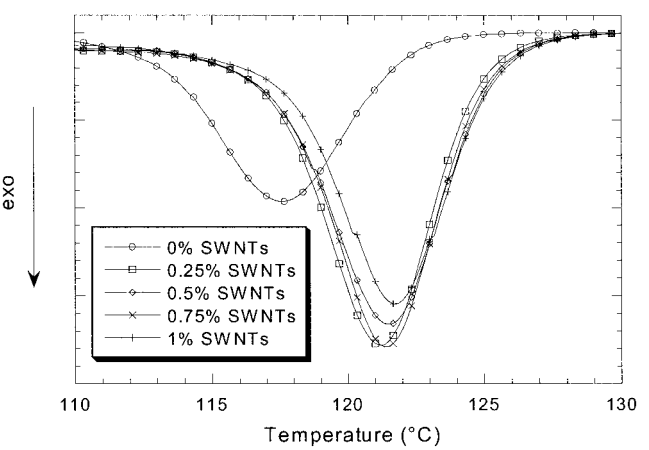

Figure 3 Nonisothermal crystallization curves of PP–EPDM and PP–EPDM/SWNT composites.

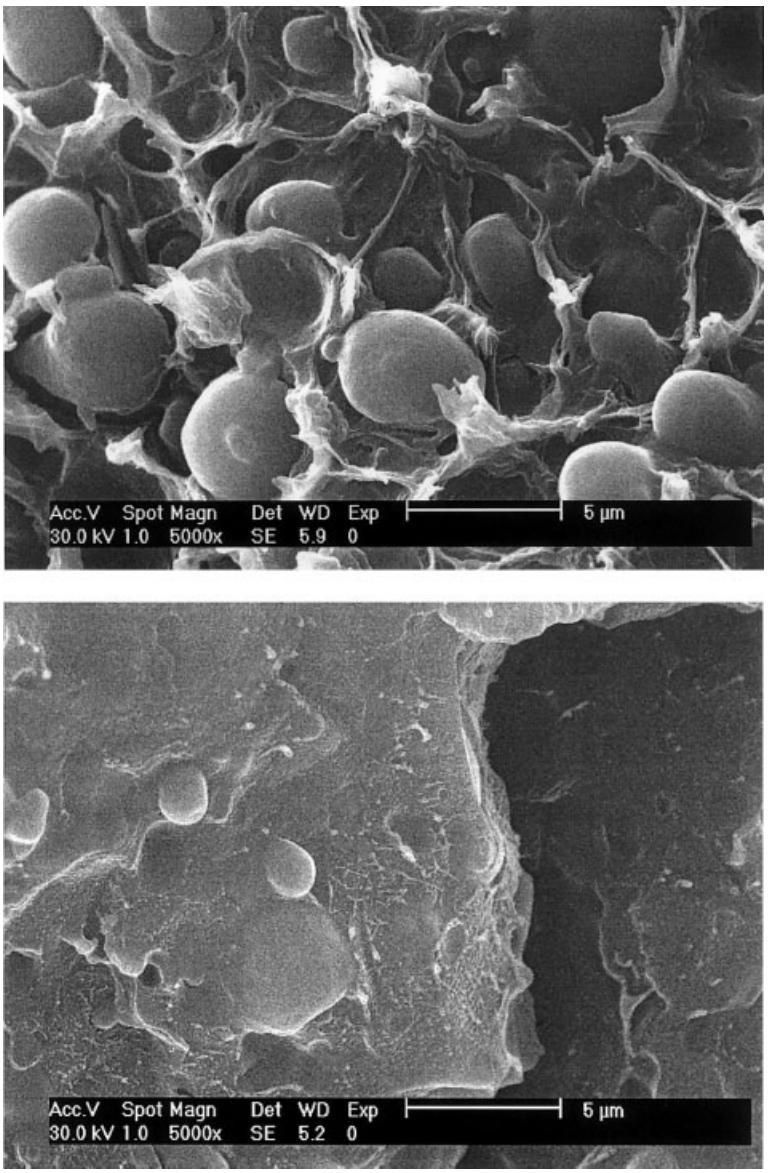

Figure 4 SEM images of (a) neat PP, (b) 0.5%, (c) 1% PP–EPDM/SWNT composites, and (d) higher magnification on a 1% PP–EPDM/SWNT composite showing SWNT bundles.

Figure 5 shows the storage moduli of the PP–EPDM blend and its nanocomposites reinforced with SWNTs. The storage modulus of PP–EPDM is increased by the stiffening effect of the nanotubes, which is particularly significant at a SWNT concentration of 0.5%, rather than a nanotube concentration of 1% where the storage modulus decreases, showing a lower value than that measured for the pristine PP–EPDM polymer matrix. In addition, the ratio of the modulus at 40°C to that at −80°C is only 0.25 for PP–EPDM, but 0.32 for the composite containing 0.5% nanotubes (Fig. 6), with a sudden decrease upon an increase of nanotube concentration to 1%. These results can be explained by the fact that because of the high surface area of carbon nanotubes, when the concentration of SWNTs in the nanocomposite is increased (1%), there is no available polymer for intercalating into the bundles. As a consequence, the interactions between the nanotubes are higher, giving rise to the formation of aggregates responsible for the decrease of the mechanical properties. This behavior was recently reported and related to the waviness of carbon nanotubes.[18]

The tan δ curves of the composites are reported in Figure 7. The tan δ peak moves to a slightly higher temperature with increasing nanotube contents, showing that the glass-transition temperature of the composite is increased by the addition of nanotubes. In other words, nanotubes hinder the segmental motion of the PP–EPDM chains.

Raman characterization was also applied to highlight the effects of SWNTs on the PP–EPDM matrix composites. The Raman spectra recorded on the com-

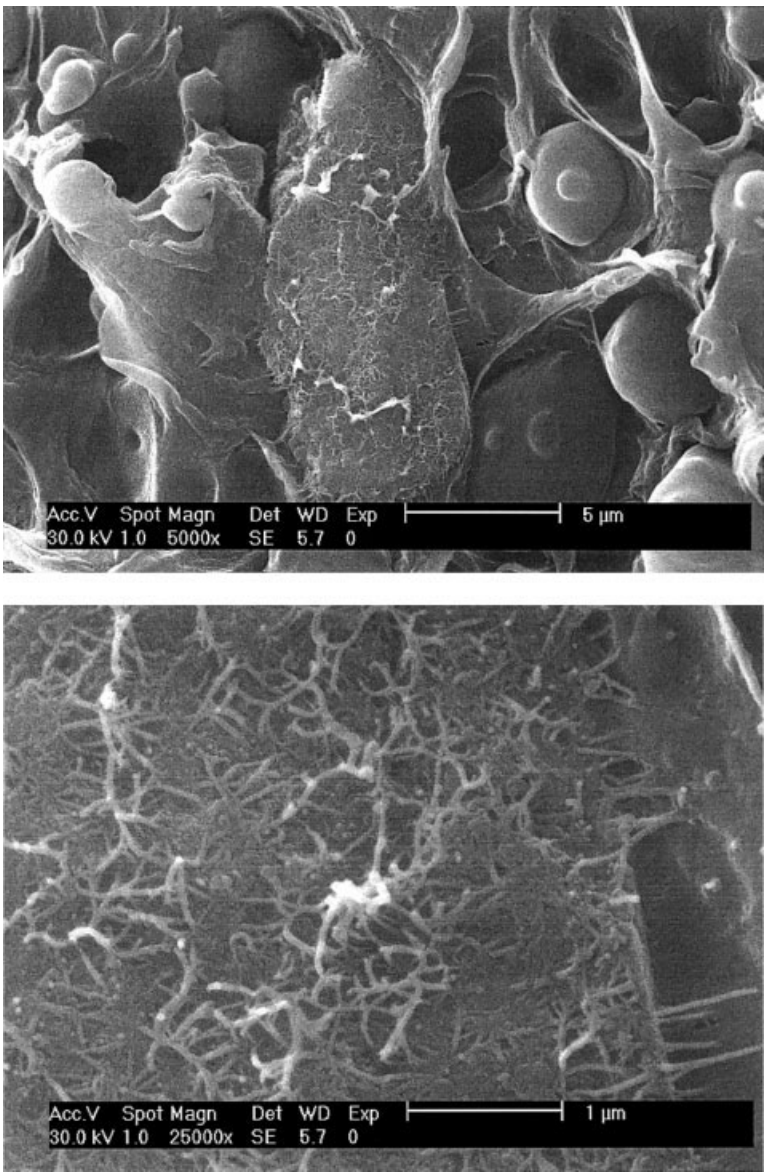

Figure 4 (*Continued from the previous page*)

posites with several SWNT concentrations (0.25, 0.5, 0.75, and 1%) in the low-frequency segment (Fig. 8) show a well-pronounced peak at around 100–200 cm^{-1}. This band is attributed to the breathing mode A_{1g} of nanotubes and its frequency depends on the inverse diameter.[19–30] The spectra were then analyzed quantitatively by searching the minimum number of frequencies that fitted the different Raman bands without fixing the position and the widths of the individual peaks. By using the fitting procedure explained above, three main features appear in the PP–EPDM/SWNTs spectra at 145, 160, and 200 cm^{-1}. From Figure 9, it is clear that the aforementioned peaks are upshifted when a low concentration of nanotubes is introduced to the PP–EPDM. We notice that the shift in frequency of the feature depends on the nanotube diameter. The lower frequencies, which correspond to the higher diameters, are more shifted than the higher ones.

The observed changes of PP–EPDM crystallization are certainly a result of microstructural changes induced by the incorporation of SWNTs. Each peak from the decomposition of the low-frequency bands can be attributed to the nanotube bundle dimension. When the nanotubes are incorporated into the polymer, the low phonon band positions are shifted toward higher frequencies (Fig. 9), especially the lower frequency peaks; the observed shifts then can be explained by the effects of intercalation of the polymer into bundles. In fact, the polymer exerts a pressure on the individual tubes, thus increasing the breathing mode frequencies. Furthermore, in the low-concentration samples, the quantity of PP–EPDM intercalated between the nanotubes could lead to an opening of the bundles, enhanc-

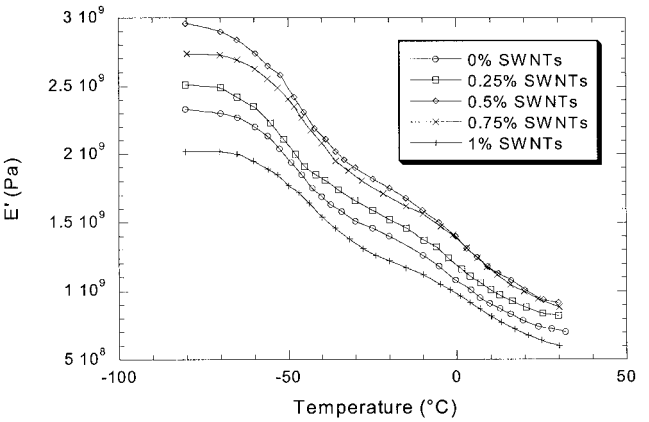

Figure 5 Storage moduli of PP–EPDM and PP–EPDM/SWNT composites.

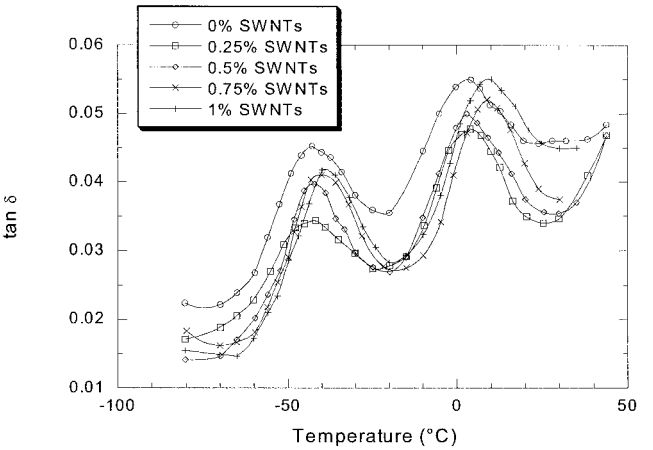

Figure 7 Tan δ peaks of PP–EPDM and PP–EPDM/SWNT composites.

ing the formation of nucleant agents to favor the crystallization process.

Thus, the behavior of the features at 145 and 200 cm^{-1} shows two extreme situations. For low nanotube concentrations, an intercalation of the polymer inside SWNT bundles is allowed, leading to an increase in nanotube dispersion. Thus, interactions between nanotubes are low and the bundles can be desegregated. At higher nanotube concentrations, the structure of the bundles seems unchanged and the quantity of aggregates increases with an increase in nanotube concentration, preventing further intercalation of the polymer.

CONCLUSIONS

The physical and mechanical properties of single-walled carbon nanotube reinforced ternary composites based on blends of polypropylene (PP) and ethylene–propylene–diene rubber (EPDM) were analyzed in the present work. It was demonstrated how the incorporation of SWNTs affects the crystalline behavior and structure of the PP matrix and how this change is very important to interpret the function of the nanotubes as a reinforcement in composite materials. In particular, SWNTs accelerate the nucleation and crystal growth mechanisms of PP, an effect that is more appreciable at low nanotube contents (0.25%). This effect is attributed to the intercalation of a high quan-

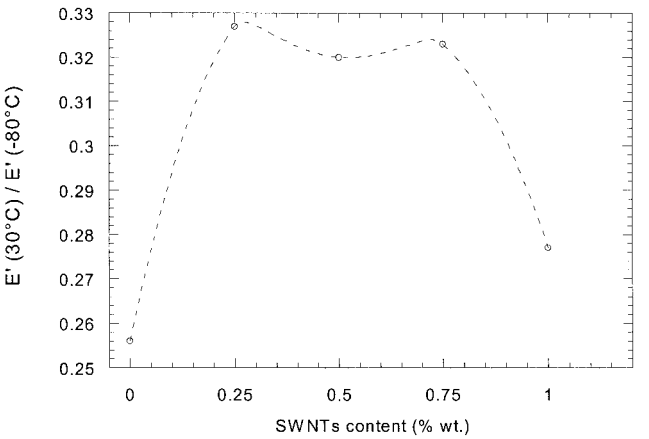

Figure 6 E' (40°C)/E' (−80°C) ratios of PP–EPDM and PP–EPDM/SWNT composites.

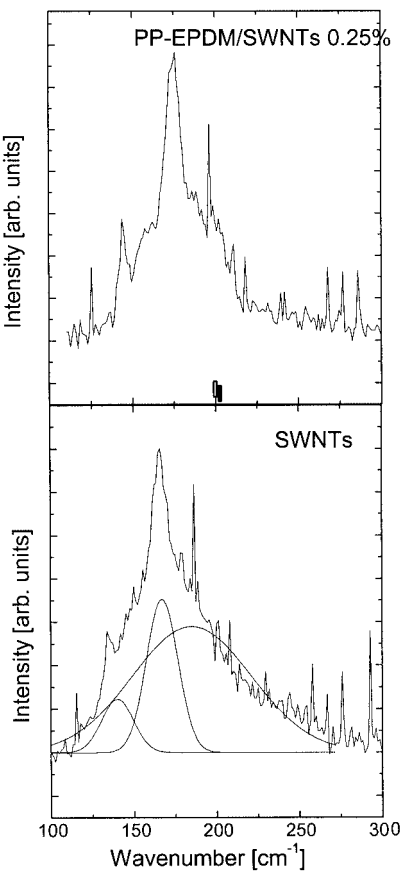

Figure 8 Low-frequency Raman spectra of SWNTs and PP–EPDM/SWNT composites.

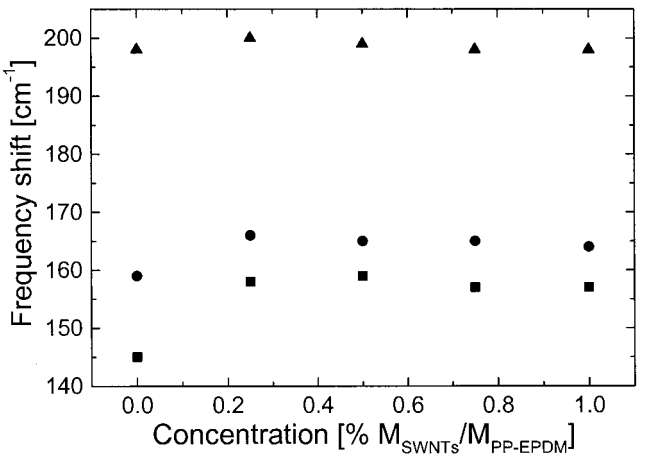

Figure 9 Decomposition of the low frequency bands of PP–EPDM/SWNT composites for several concentrations.

tity of polymer between SWNTs into bundles, leading to a higher dispersion and offering a higher surface for crystal nucleation. Dynamic mechanical analysis confirmed the reinforcing effects of the nanotubes for these systems based on PP–EPDM blends. In fact, the incorporation of low concentrations of SWNTs gives rise to a more rigid material, which is reflected in a marked increase of the storage modulus. This effect is not noticeable at the highest nanotube content in the blend. These results find an explanation in terms of microstructural changes evidenced by Raman spectroscopy. The changes of the low-frequency Raman bands demonstrate that, for the low nanotube concentration, the polymer is intercalated between nanotubes into bundles that can be disaggregated. On the other hand, when the nanotube concentration is high, the high quantity of nanotubes does not allow the intercalation of a high quantity of polymers between SWNTs into bundles.

References

1. Iijima, S. Nature 1991, 354, 56.
2. Rinzler, A. G.; Hafner, J. H.; Nikolaev, P.; Lou, L.; Kim, S. G.; Tomanek, D.; Nordander, P.; Cobert, D. T.; Smalley, R. E. Science 1995, 269, 1550.
3. De Heer, W. A.; Chatelain, A.; Ugarte, D. Science 1995, 270 1179.
4. Collins, P. G.; Zettl, A.; Bando, H.; Thess, A.; Smalley, R. E. Science 1997, 278, 100.
5. Wagner, H. D.; Lourie, O.; Feldman, Y.; Tenne, R. Appl Phys Lett 1998, 72, 188.
6. Dagani, R. Chem Eng News 1999, 7, 25.
7. Wang, Z. L.; Poncharal, P.; de Heer, W. A. In: Proceedings of the First IUPAC Workshop on Advanced Materials: Nanostructured Systems, Hong Kong, July 14–18, 1999.
8. Curran, S.; Ajayan, P.; Blau, W.; Carrol, D.; Coleman, J.; Dalton, A.; Davey, A. P.; McCarthy, B.; Stevens, A. Adv Mater 1998, 10, 1091.
9. Alexandre, M.; Dubois, P. Mater Sci Eng 2000, 28, 1.
10. Hoshino, S.; Meinecke, E.; Power, J.; Stein, R.; Newman, S. J Polym Sci 1995, 3, 3041.
11. Bisbergen, F. L.; DeLange, B. Polymer 1970, 11, 309.
12. Pratt, C. F.; Hobbs, S. Y. Polymer 1976, 17, 12.
13. Martuscelli, E.; Pracella, M.; Volpe, G. D.; Greco, P. Makromol Chem 1984, 185, 1041.
14. Jammak, J.; Cheng, S.; Zhang, A.; Hsieh, E. Polymer 1992, 33, 728.
15. Synnott, D. J.; Sheridan, D. F.; Kontos, E. G. In: Thermoplastic Elastomers from Rubber-Plastic Blends; De, S. K., Bhowmick, A. K., Eds.; Ellis Horwood: New York, 1990.
16. Hoppner, D.; Wendorff, J. H. Colloid Polym Sci 1990, 268, 500.
17. Karger-Kocsis, J.; Csiku, I. Polym Eng Sci 1987, 27, 24.
18. Menard, K. P. Dynamic Mechanical Analysis: A practical Introduction; CRC Press: Boca Raton, FL, 1999.
19. Dresselhaus, M. S.; Eklund, P. C. Adv Phys 2000, 49, 705.
20. Rao, A. M.; Jorio, A.; Pimenta, M. A.; Dantas, M. S.; Saito, R.; Dresselhaus, G.; Dresselhaus, M. S. Phys Rev Lett 2000, 84, 1820.
21. Brown, S. D.; Jorio, A.; Dresselhaus, G.; Dresselhaus, M. S. Phys Rev B 2001, 64, 73403.
22. Bandow, S.; Asaka, S.; Saito, Y.; Rao, A. M.; Grigorian, L.; Richter, E.; Eklund, P. C. Phys Rev Lett 1998, 80, 3779.
23. McNamara, K. M.; Williams, B. E.; Gleason, K. K.; Scruggs, B. E. J Appl Phys 1994, 76, 2466.
24. de la Chappelle, M. L.; Lefrant, S.; Journet, C.; Maser, W.; Bernier, P.; Loiseau, A. Carbon 1998, 36, 705.
25. Eklund, C.; Holden, J. M.; Jishi, R. A. Carbon 1995, 33, 959.
26. Rao, A. M.; Richter, E.; Bandow, S.; Chase, B.; Eklund, P. C.; Williams, K. A.; Fang, S.; Subbaswamy, K. R.; Menon, M.; Thess, A.; Smalley, R. E.; Dresselhaus, G.; Dresselhaus, M. S. Science 1997, 275, 187.
27. Rinzler, A. G.; Liu, J.; Dai, H.; Nikolaev, P.; Huffman, C. B.; Rodriguez-Macias, F. J.; Boul, P. J.; Lu, A. H.; Heymann, D.; Colbert, D. T.; Lee, R. S.; Fischer, J. E.; Rao, A. M.; Eklund, P. C.; Smalley, R. E. Appl Phys A 1998, 67, 29.
28. Iliev, M. N.; Litvinchuk, A. P.; Arepalli, S.; Nikolaev, P.; Scott, C. D. Chem Phys Lett 2000, 316, 217.
29. Pimenta, M. A.; Marucci, A.; Brown, S. D. M.; Mattews, M. J.; Rao, A. M.; Eklund, P. C.; Smalley, R. E.; Dresselhaus, G.; Dresselhaus, M. S. J Mater Res 1998, 13, 2396.
30. Valentini, L.; Biagiotti, J.; Kenny, J. M. J Appl Polym Sci 2003, 87, 708.